Heliyon 8 (2022) e12033

Contents lists available at ScienceDirect

Heliyon

journal homepage: www.cell.com/heliyon

Research article

Development and application of a new sensitivity analysis model for the remote sensing retrieval of heavy metals in water

Yu Guo [a], Ruru Deng [a,b,**], Jiayi Li [a], Jing Wang [a], Zhenqun Hua [a], Yuming Tang [a], Yeheng Liang [a,*,1]

[a] School of Geography and Planning, Sun Yat-Sen University, Guangzhou 510006, China
[b] Guangdong Engineering Research Center of Water Environment Remote Sensing Monitoring, Guangzhou 510006, China

HIGHLIGHTS

- A new remote sensing sensitivity model (the D-δ(ε) model) for analysing heavy metals in water is proposed.
- The mathematical relationship between retrieved remote sensing concentrations and radiometric resolution is revealed.
- The curve showing the lowest detectable concentrations using remote sensing retrieval methods is obtained.
- This work proves to the academic community the feasibility of applying remote sensing techniques to heavy metals in water.

ARTICLE INFO

Keywords:
Sensitivity analysis method
Remote sensing retrieval
Heavy metal pollution

ABSTRACT

This work proposes a new sensitivity analysis model, referred to as the D-δ(ε) model, for the remote sensing retrieval of heavy metals in bodies of water. By defining the reflectance ratio function (δ(ε)), we deduce the mathematical relationships between the heavy metal concentration sequences (D_i) that can be effectively used for remote sensing retrievals and the radiometric resolution (ε) of the remote sensing instrument. Then, as a function of wavelength, we obtain the curve of the lower limit of the heavy metal concentrations in water that can be retrieved by remote sensing. To demonstrate the advantages of this model, we take two compounds, copper sulphate ($CuSO_4$) and cadmium sulphide (CdS), as examples to discuss the remote sensing sensitivity of different wavelengths when retrievals are performed using the Chinese HJ-1A's hyperspectral imager (HSI). The results showed that the lowest detectable concentration of $CuSO_4$ in the wavelength range of 460.04–496 nm (corresponding to bands 1–17 of the HSI image) can be below 0.15 mg/L, while the concentration of CdS can be lower than 0.001 mg/L in the separate ranges of 460.04–493.59 nm (bands 1–16) and 526.885–594.79 nm (bands 29–51). This model clearly demonstrates the mathematical relationship obeyed by "D-ε". Additionally, this model can not only calculate the retrieval concentration sequences at any observation wavelength but also intuitively provide the curve of the lower concentration limit for heavy metal retrievals. This work provides a theoretical basis for the selection of the most sensitive bands for remote sensing retrieval using hyperspectral images in the future.

1. Introduction

Retrieving the concentrations of heavy metals in water by remote sensing techniques has been a persistent and difficult problem in the field of environmental remote sensing. The possibility of remotely sensing heavy metals in water was first proposed in 2010 by Chen et al. [1]. The statistical relationship between the measured data and the remote sensing reflectance was established, and a preliminary experiment was carried out to quantify the concentrations of several common heavy metals from remotely sensed data in the Pearl River Estuary [1, 2, 3]. Additionally, Liang et al. used Deng's model to conduct remote sensing retrieval research on copper and iron in the Beijiang River [4]. However,

* Corresponding author.
** Corresponding author.
E-mail addresses: eesdrr@mail.sysu.edu.cn (R. Deng), liangyeheng@163.com (Y. Liang).
[1] Co-first author, this author contributed equally to this work.

https://doi.org/10.1016/j.heliyon.2022.e12033
Received 2 August 2022; Received in revised form 21 October 2022; Accepted 24 November 2022

the above research remains in the exploratory stage. Once they had recognized the lack of optical parameters required by remote sensing models, the limited research on the spectral characteristics of heavy metal polluted water, and the lack of sensitivity analyses, Liang and Deng began fundamental research. This included, identifying the optical parameters of heavy metal compounds [5, 6, 7], analysing the spectral characteristics of typical heavy metal polluted water and the determining retrieval method of these optical parameters [8, 9]. The intent of that work was to improve the theoretical foundation of the field, to ensure the effective use of remotely sensed satellite images for analysing heavy metal concentrations.

However, since the beginning of this field over ten years ago, there have been few advancements in the use of remote sensing images to determine the concentrations of heavy metals from water. In addition to the limitations mentioned above, a central reason for the challenges involved in measuring heavy metals concentrations from satellite platforms is that the heavy metal concentration of natural water is usually very low, albeit potentially fatal to humans. These concentrations are considered too low to be adequately observed in remote sensing images or ground-based spectral measurement data. The feasibility of applying remote sensing retrieval methods in this context has since been questioned and has become a further hindrance that has restricted the development of this field. In order to address these issues, it is necessary to first conduct a sufficient feasibility or sensitivity analysis.

We know that a sensitivity analysis (SA) is an important part of improving, or selecting, suitable remote sensing model parameters. There are many studies in this field, and the main methods and principles used are as follows: (1) Design different sensitivity indicators (SI) used for qualitative analysis through statistical methods; (2) Develop techniques in accordance with the physical relationship between the parameters of the remote sensing model and SI.

The first method types assess the sensitivity of the remote sensing model parameters during the retrieval by calculating the statistical relationship between the changes in the model input parameters and the corresponding changes in the retrieval results. The most common analysis algorithms are the Morris Screening Method (Morris), Sobol's Method (Sobol) and the Standardized Regression Coefficient (SRC) [10, 11]. For example, Yi et al. [12] and Wang et al. [13] applied the Morris method to analyse the sensitivity of the Environmental Fluid Dynamic Code (EFDC) model parameters to nitrogen and the sensitivity of the environmental characteristics in Dianchi Lake and Chaohu Lake to phosphorus. Li et al. [14] combined the K-means clustering algorithm and the Morris method to analyse the spatial sensitivity of the parameters of the algal retrieval model. Liu et al. [15] applied the Sobol algorithm to analyse the sensitivity of the water parameters, sediment parameters, meteorological conditions and input boundaries in the Intelligent Watershed Integration Decision (IWIND) model to nitrogen and phosphorus in Dianchi Lake. Vanrolleghem et al. [16] and Ikumi [17] applied the SRC method to analyse the parameter sensitivity of an urban water resource model and a water environment model. Furthermore, they define different SIs to compare only the variation between the changes in the input parameters of the remote sensing model and the corresponding changes in the retrieval results to analyse the parameter sensitivity of the remote sensing model [18, 19, 20, 21, 22]. For example, Privette et al. [23] defined the parameter sensitivity (S) to perform sensitivity analyses on different directions of the bidirectional reflectance distribution function (BRDF) model. Li and Yao [24, 25] improved the parameter S and proposed the uncertainty and sensitivity matrix (USM) to describe the sensitivity of the BRDF model in each sampling direction. Hosseini et al. [26] and Chen et al. [27] applied the one-factor-at-a-time (OAT) method to define SI and analysed the sensitivity of the water quality model parameters to nitrogen in the Large Prairie River and Danjiangkou Reservoir. The above studies establish various sensitivity evaluation methods from a statistical perspective, which are simple and easy to implement, but the analysis results usually only have statistical significance and cannot reveal the intrinsic physical relationship between model parameters and sensitivity indicators.

The second type of method is much more difficult to model and solve than the first type of method. Ustinov [28, 29, 30] applied this method and proposed an adjoint sensitivity matrix approach for application in atmospheric models, which provided the temperature and gas mixing ratio weighting functions for atmospheric remote sensing based on thermal infrared scattering. This method does not overly rely on statistical indicators but starts from the mechanisms that influence the relationship between the atmospheric model and its sensitivity, thus, providing a more quantitative sensitivity evaluation method.

In summary, the conventional thinking of scholars regarding the sensitivity of remote sensing models was to qualitatively evaluate the influence of parameters on the model based on statistical indicators. Individual scholars used the modelling principles of the remote sensing models, which could further quantify this sensitivity indicator. The main purpose of their research was to more effectively improve the accuracy of existing remote sensing models through sensitivity analysis rather than to examine the feasibility of retrieval parameters. However, as the most direct and reliable physical quantity that reflects the sensitivity of remote sensing instruments, the mathematical relationship between the radiometric resolution and the concentration of heavy metals in water has not been studied. The concentration of heavy metals in water presented in this paper reflects the uncertainty in the relationship between the lower limits of the remote sensing retrieval of that concentration and the radiometric resolution of the instrument. This uncertainty leads to the incorrect assertion that the technique application itself is not feasible; thus, research has progressed slowly.

Therefore, this study focuses on building a quantitative evaluation model that can be used for remote sensing sensitivity analyses and can reveal the inherent relationship between radiometric resolution and heavy metal concentration.

2. Theory and data

2.1. Model construction

2.1.1. Model assumptions and definitions

To more rigorously express and deduce the mathematical relationship between the aqueous concentration of a certain heavy metal and the radiometric resolution of the sensor, we need to make conditional a priori assumptions and establish certain definitions.

Model assumption: The change in the brightness value of the remote sensing image pixel, or digital number (DN), is only caused by the change in the concentration of one component within the water, such as one species of heavy metal.

Definition (1): For the observation wavelength (λ), the relationship between the concentration of a certain heavy metal in water (D_n) and the surface reflectance of the Earth (r_n) can be expressed as the following function:

$$r_n = f_1(D_n) \tag{1}$$

The relationship between planetary reflectance (R_n) and surface reflectance of the Earth (r_n) can be expressed as follows:

$$R_n = f_2(r_n) \tag{2}$$

Substituting Eq. (1) into Eq. (2), we obtain:

$$R_n = f_2[f_1(D_n)] \tag{3}$$

where f_1 is the specific expression of the water quality remote sensing retrieval model and f_2 is the specific expression of the atmospheric correction model. For simplicity, a function of wavelength (λ) will be expressed without λ. For example, $R(\lambda)$ will be written as R.

For ground spectrometers, atmospheric effects can be ignored, and Eq. (3) can be simplified as:

$$R_n = f_1(D_n) \tag{4}$$

Definition (2): For the observation wavelength (λ), the function δ of the reflectance R_a and R_b of any two concentrations D_a and D_b of a certain heavy metal in water, can be define as follows:

$$\delta_{b-a} = R_a / R_b \tag{5}$$

It is stipulated here that D_b is always greater than D_a; that is, we consider that D_a is the concentration before the change, D_b is the concentration after the change, and the subscript also satisfies that $b > a$. From Eq. (3), the function δ is also a function of concentration (D), and δ is always positive.

Definition (3): For the observation wavelength (λ), the DN value (DN_i) of the remote sensing image should be a sequence of integers from 0 to $(2^m - 1)$, where $i = 0, 1, 2, \cdots$; m is the number of bits in the remote sensing data. For example, the Chinese HJ-1A hyperspectral imager (HSI) image is in 16-bit format, thus, the range of the DN values includes all integers from 0 to $(2^{16} - 1)$.

It is stipulated here that $i = 0$ refers to the background value DN_0. When $D_0 = 0$, $DN_0 \in (0, 2^m - 1)$ and $DN_0 \in N$. Usually, the value of DN_0 is found elsewhere within the range and does not take the boundary value (see Figure 1).

Definition (4): If the DN value of the remote sensing image changes from DN_a to DN_b, then we suspect that the concentration of heavy metals in the water is caused by the change from D_a to D_b. Obviously, the amount of change, ΔDN_{b-a}, must be $(b-a)$ proportional with the radiometric resolution ε, namely:

$$DN_a - DN_b = \Delta DN_{b-a} = (b-a) \cdot \varepsilon \tag{6}$$

In particular, when $a = n$ and $b = n+1$ in Eq. (6), the concentration of heavy metals in water is changed from the original D_n to D_{n+1}, and the change in the DN value of the remote sensing image is:

$$DN_n - DN_{n+1} = \Delta DN_1 = (n+1-n) \cdot \varepsilon = \varepsilon \tag{7}$$

where n is a natural number, and we used the subscripts n and $n+1$ to denote any two adjacent elements.

In particular, when $a = 0$ and $b = n$ in Eq. (6), namely:

$$DN_n = DN_0 - n \cdot \varepsilon \tag{8}$$

It is stipulated here that when ε is positive, the DN decreases by ε; when ε is negative, the DN value also increases by ε (see Figure 1).

Eq. (7) is regarded as the recursion formula of the DN sequences, and Eq. (8) is regarded as the formula of the general term of the DN sequences.

In Eq. (8), $|\varepsilon|$ is the value of radiometric resolution, that is, the minimum difference between two spectral frequencies that the remote sensing sensor can distinguish. For ground spectrometers, the radiometric resolution (equivalent noise radiation) of the instrument given by the manufacturer is usually reflected in the radiance (L) and not the DN value. Atmospheric effects are not considered. However, since the derivation of the formula is similar, the following example considers only the satellite sensor.

2.1.2. Mathematical relationship between the δ function and the radiometric resolution (δ-ε Model)

According to the common methods of preprocessing remote sensing images, the conversion from the remotely sensed DN_i to the planetary reflectance (R_i) can be expressed as follows:

$$R_i = \pi L_i d^2 / (E_s \cos\theta_z) = \pi(Gain \cdot DN_i + Offset) d^2 / (E_s \cos\theta_z) \tag{9}$$

where E_s is solar irradiance on the top of the atmosphere, with units $W \cdot m^{-2} \cdot \mu m^{-1}$; θ_z is solar zenith angle; d is Sun-Earth mean distance factor; L_i is radiance, in $W \cdot m^{-2} \cdot sr^{-1} \cdot \mu m^{-1}$; $Gain$ is the sensor calibration slope in $W \cdot m^{-2} \cdot sr^{-1} \cdot \mu m^{-1}$; $Offset$ is the sensor absolute scaling factor offset in $W \cdot m^{-2} \cdot sr^{-1} \cdot \mu m^{-1}$, for certain types of remote sensing data, the value is 0. Eq. (9) is the radiometric calibration and correction model for the remote sensing images. For additional information see https://www.usgs.gov/media/files/landsat-7-data-users-handbook Page 79, Sections "5.6.5, Conversion to Radiance" and "5.6.6 Radiance to Reflectance".

According to Eq. (9), the planetary reflectance under any two concentrations of D_a and D_b can be expressed as:

$$R_a = \pi(Gain \cdot DN_a + Offset) d^2 / (E_s \cos\theta_z) \tag{10}$$

$$R_b = \pi(Gain \cdot DN_b + Offset) d^2 / (E_s \cos\theta_z) \tag{11}$$

By substituting Eq. (8) Eqs. (10) and (11), we obtain:

$$R_a = \pi[Gain \cdot (DN_0 - a \cdot \varepsilon) + Offset] d^2 / (E_s \cos\theta_z) \tag{12}$$

$$R_b = \pi[Gain \cdot (DN_0 - b \cdot \varepsilon) + Offset] d^2 / (E_s \cos\theta_z) \tag{13}$$

According to definition (2), substituting Eqs. (12) and (13) into Eq. (5), yields:

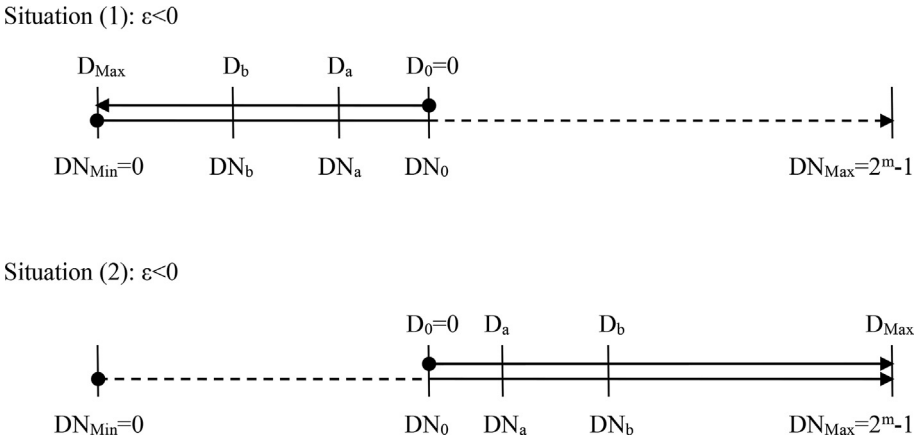

Figure 1. Correspondence between sequences DN_i and D_i.

$$\delta_{a-b}=\frac{R_b}{R_a}=\frac{Gain\cdot(DN_0-b\cdot\varepsilon)+Offset}{Gain\cdot(DN_0-a\cdot\varepsilon)+Offset}=\left[1-\frac{Gain\cdot(a-b)\cdot\varepsilon}{Gain\cdot(DN_0-b\cdot\varepsilon)+Offset}\right]^{-1} \tag{14}$$

For the ground spectrometer, DN conversion is not needed, thus, $Gain=1$ W/m^2/sr/μm and $Offset=0$ W/m^2/sr/μm, that is, $DN_0 = L_0$.

For subsequent disambiguation, we denote Eq. (14) as $\delta_{a-b}(\varepsilon,a,b)$ to show that it is a function of the radiometric resolution and the variable sequence subscript.

In particular, considering the condition of two adjacent concentrations, and letting the subscripts be $a=n+1$ and $b = n$, Eq. (14) becomes:

$$\begin{aligned}\delta_{(n+1)-n}(\varepsilon,n+1,n)=\delta_1(\varepsilon,n+1,n)&=\frac{R_n}{R_{n+1}}=\frac{Gain\cdot(DN_0-n\cdot\varepsilon)+Offset}{Gain\cdot[DN_0-(n+1)\cdot\varepsilon]+Offset}\\&=\left[1-\frac{Gain\cdot\varepsilon}{Gain\cdot(DN_0-n\cdot\varepsilon)+Offset}\right]^{-1}\end{aligned} \tag{15}$$

Considering when Eq. (14) when the subscripts $a=n$ and $b = 0$, we obtain:

$$\begin{aligned}\delta_{n-0}(\varepsilon,n,0)=\delta_n(\varepsilon,n,0)&=\frac{R_0}{R_n}=\frac{Gain\cdot(DN_0-0\cdot\varepsilon)+Offset}{Gain\cdot[DN_0-n\cdot\varepsilon]+Offset}\\&=\left(1-\frac{Gain\cdot n\cdot\varepsilon}{Gain\cdot DN_0+Offset}\right)^{-1}\end{aligned} \tag{16}$$

Eq. (16) represents the general term of the function $\delta(\varepsilon,n,0)$ sequences.

2.1.3. Mathematical relationship between concentration and radiometric resolution (the D-δ(ε) model)

According to definition (1), when the reflectance values for R_a and R_b, that correspond to any two concentrations D_a and D_b, are substituted into Eq. (5), we obtain:

$$\delta_{b-a}(\varepsilon,b,a)=R_a/R_b=f_2[f_1(D_a)]/f_2[f_1(D_b)] \tag{17}$$

Once the water quality remote sensing model f_1 and atmospheric correction model f_2 in Eq. (17) are determined, the relationship between any two concentrations D_a and D_b can be presented as:

$$D_b=g[D_a,\delta_{b-a}(\varepsilon,b,a)] \tag{18}$$

From Eq. (18), after the specific forms of f_1 and f_2 are given, g can be determined, and we will give the specific f_1 in Section 2.2.1.

In particular, according to Eq. (18), and letting the subscripts be $a=n$ and $b = n+1$, we obtain:

$$D_{n+1}=g\left[D_n,\delta_{(n+1)-n}(\varepsilon,n+1,n)\right]=g[D_n,\delta_1(\varepsilon,n+1,n)] \tag{19}$$

where function δ from Eq. (19) is expressed by Eq. (15).

From Eq. (18), and letting the subscripts be $a=0$ and $b = n$, we obtain:

$$D_n=g[D_0,\delta_{n-0}(\varepsilon,n,0)]=g[D_0,\delta_n(\varepsilon,n,0)] \tag{20}$$

where $D_0 = 0$; δ function in Eq. (20) is expressed by Eq. (16).

Eq. (20) defines the general term of the concentration sequences (D_i), which denotes the functional relationships between concentration and radiometric resolution, and thus, is the **D-δ(ε) model** proposed in this work.

Obviously, if the water does not contain heavy metals at the beginning, then $D_0 = 0$ and regardless of Eq. (19) or (20), the following can be obtained:

$$D_1=g[D_0,\delta_{1-0}(\varepsilon,1,0)]=g[0,\delta_1(\varepsilon,1,0)] \tag{21}$$

Furthermore, regardless of Eq. (15) or (16), the δ function in Eq. (21) becomes:

$$\begin{aligned}\delta_{1-0}(\varepsilon,1,0)=\delta_1(\varepsilon,1,0)&=\left[1-\frac{Gain\cdot(1-0)\cdot\varepsilon}{Gain\cdot(DN_0-0\cdot\varepsilon)+Offset}\right]^{-1}\\&=\left(1-\frac{Gain\cdot\varepsilon}{Gain\cdot DN_0+Offset}\right)^{-1}\end{aligned} \tag{22}$$

2.2. Application data

Next, we use the D-δ(ε) model constructed in Section 2.1, which is applied to a case of simulated clear and deep water that ignores the influence of the atmosphere. Obviously, these calculation results will be lower than those obtained from actual imagery, but this determines the minimum concentration that can theoretically be extracted by remote sensing for a certain heavy metal. Similar principles and methods hold true for future practical application.

2.2.1. Determination of function f_1

In Eq. (4), f_1 represents a remote sensing model based on radiative transfer theory [31], and does not considering the reflected light from the bottom of the waterbody, secondary scattering or atmospheric effects. Eq. (4) can be expanded as:

$$R_n=f_1(D_n)=P(\Theta)(B+D_n\beta_{HM})/[4\mu(K+D_nk_{HM})] \tag{23}$$

where $P(\Theta)$ is the scattering phase function, Θ is the scattering angle, and $P(\Theta) = 3[1+\cos^2(\Theta)]/4$; μ is the observation geometry factor; β_{HM} is the scattering coefficient of the heavy metal; k_{HM} is the extinction coefficient of the heavy metal; and B and K represent the total scattering coefficient and total extinction coefficient of the other components in the background water except the heavy metal.

Substituting Eq. (23) into Eq. (19) yields:

$$D_{n+1}=g[D_n,\delta_1(\varepsilon,n+1,n)]=\frac{\delta_1(\varepsilon,n+1,n)\cdot B\cdot(K+D_n\cdot k_{HM})-K\cdot(B+D_n\cdot\beta_{HM})}{k_{HM}\cdot(B+D_n\cdot\beta_{HM})-\delta_1(\varepsilon,n+1,n)\cdot\beta_{HM}\cdot(K+D_n\cdot k_{HM})} \tag{24}$$

Where the δ function of Eq. (24) is expressed by Eq. (15).

When $n = 0$, $D_0 = 0$. Similarly, Eq. (21) can be expanded as:

$$D_1=g[0,\delta_1(\varepsilon,1,0)]=\frac{\delta_1(\varepsilon,1,0)\cdot B\cdot K-K\cdot B}{k_{HM}\cdot B-\delta_1(\varepsilon,1,0)\cdot\beta_{HM}\cdot K}=\frac{\delta_1(\varepsilon,1,0)-1}{k_{HM}/K-\delta_1(\varepsilon,1,0)\cdot\beta_{HM}/B} \tag{25}$$

where the δ function in Eq. (25) is expressed by Eq. (22).

Eq. (20) can be expanded as:

$$D_n=g[D_0,\delta_n(\varepsilon,n,0)]=\frac{\delta_n(\varepsilon,n,0)-1}{k_{HM}/K-\delta_n(\varepsilon,n,0)\cdot\beta_{HM}/B} \tag{26}$$

where δ in this instance is expressed by Eq. (16).

According to Eq. (9), the background DN value (DN_0) of the remote sensing image in Eqs. (15), (16), and (22) can be calculated by the following formula:

$$DN_0=\left[R_0E_s\cos\theta_z/(\pi d^2)-Offset\right]/Gain \tag{27}$$

2.2.2. Set the parameters of the D-δ(ε) Model

After Eqs. (27) and (16) are substituted into Eq. (26), the concentration sequences (D_i) can be calculated. Eq. (26) mainly

Table 1. Satellite sensor parameter settings for the D-δ(ε) model.

Parameter Name	Parameter Symbol	Value
Satellite platform	\	HJ-1A of China
Sensor	\	Hyperspectral imager (HSI)
Observation wavelength range	λ_i, (i = 1,2,…,115)	460–950nm (115 bands), more detail in Table 2.
Date of image	\	December 26th, 2013
Observation zenith angle	θ_v	0° (vertical observation), obtained from satellite data header file.
Solar elevation angle	θ_s	31.554°, obtained from satellite data header file.
Solar zenith angle	θ_z	Calculate with the following formula: $\theta_z = 90° - \theta_s$
Scattering angle	Θ	Calculate with the following formula: $\Theta = 180° - \theta_z$
Observation geometry factor	μ	Calculate with the following formula: $\mu = \sec\theta_z + \sec\theta_v$
Sun-Earth mean distance factor	d	0.9835, obtained from permanent calendar.
Sensor calibration slope	*Gain*	0.01 $W \cdot m^{-2} \cdot sr^{-1} \cdot \mu m^{-1}$, obtained from satellite data header file.
Sensor absolute scaling factor offset	*Offset*	0 $\cdot m^{-2} \cdot sr^{-1} \cdot \mu m^{-1}$, obtained from satellite data header file.
Radiometric resolution	ε	1
Solar irradiance on the top of the atmosphere	$E_s(\lambda_i)$	Provided by the website of China Centre For Resources Satellite Data and Application.

Table 2. The band setting of the HSI sensor, where λ is the observed centre wavelength. All bands in Table 2 are effectively available.

No.	λ (nm)	No.	λ (nm)	No.	λ (nm)	No.	λ (nm)	No.	λ (nm)
Band1	460.040	Band25	516.170	Band49	587.900	Band73	682.785	Band97	814.195
Band2	462.135	Band26	518.810	Band50	591.325	Band74	687.410	Band98	820.775
Band3	464.250	Band27	521.475	Band51	594.790	Band75	692.095	Band99	827.465
Band4	466.380	Band28	524.165	Band52	598.295	Band76	696.845	Band100	834.265
Band5	468.530	Band29	526.885	Band53	601.845	Band77	701.660	Band101	841.175
Band6	470.705	Band30	529.635	Band54	605.435	Band78	706.540	Band102	848.200
Band7	472.900	Band31	532.415	Band55	609.065	Band79	711.495	Band103	855.345
Band8	475.110	Band32	535.220	Band56	612.740	Band80	716.515	Band104	862.615
Band9	477.345	Band33	538.055	Band57	616.460	Band81	721.605	Band105	870.005
Band10	479.600	Band34	540.920	Band58	620.225	Band82	726.770	Band106	877.525
Band11	481.875	Band35	543.815	Band59	624.035	Band83	732.010	Band107	885.175
Band12	484.175	Band36	546.745	Band60	627.895	Band84	737.330	Band108	892.960
Band13	486.495	Band37	549.710	Band61	631.805	Band85	742.725	Band109	900.885
Band14	488.835	Band38	552.700	Band62	635.760	Band86	748.195	Band110	908.950
Band15	491.200	Band39	555.725	Band63	639.765	Band87	753.750	Band111	917.160
Band16	493.590	Band40	558.785	Band64	643.820	Band88	759.390	Band112	925.520
Band17	496.000	Band41	561.875	Band65	647.930	Band89	765.110	Band113	934.035
Band18	498.435	Band42	565.000	Band66	652.090	Band90	770.920	Band114	942.705
Band19	500.895	Band43	568.160	Band67	656.305	Band91	776.820	Band115	951.540
Band20	503.375	Band44	571.360	Band68	660.575	Band92	782.805		
Band21	505.885	Band45	574.595	Band69	664.900	Band93	788.885		
Band22	508.420	Band46	577.865	Band70	669.285	Band94	795.065		
Band23	510.975	Band47	581.175	Band71	673.725	Band95	801.340		
Band24	513.560	Band48	584.520	Band72	678.225	Band96	807.715		

involves two types of parameters, namely, satellite sensor parameters and water component optical parameters. See Table 1 and Table 3 for details.

(1) **Satellite sensor parameters**

The following is an example of the HSI sensor of the Chinese HJ-1A satellite. Details of these parameter settings are in Table 1. The observed centre wavelengths of the HSI sensor are listed in Table 2.

(2) **Water component optical parameters**

Examples of heavy metal compounds include $CuSO_4$ and CdS. The background water condition is set as the ideal clear and deep water. Details of these parameter settings are shown in Table 3.

3. Results and discussion

3.1. Results

By setting the model parameters, as shown in Table 1 and Table 3, Eqs. (22) and (25) were used to simultaneously calculate the lower limit concentration D_1 of these two heavy metal compounds ($CuSO_4$ and CdS) as a function of wavelength (see Figures 2 and 3) from the remote sensing images. Figure 2 shows the calculation results of the $CuSO_4$ solutions. As a function of wavelength, for normal coordinates in the display range 0–800 mg/L, see Figure 2(a); for normal coordinates in the display range of 0–4 mg/L, see Figure 2(b); and for logarithmic coordinates, see Figure 2(c). Due to the large variation in the values, both the normal coordinates and the logarithmic coordinates are used for display. What interests us is the case of the low value region;

Table 3. Water component optical parameter settings for the D-δ(ε) model. The parameters in Table 3 are all functions of the wavelength. For simplicity, λ will be omitted from the function notation. For example, $R_w(\lambda)$ will be written as R_w.

Parameter Name	Parameter Symbol	Value
Absorption coefficient of water molecule	a_w	Obtained from Refs. [32, 33]
Scattering coefficient of water molecules	β_w	Obtained from Ref. [34]
Extinction coefficient of water molecule	k_w	Calculate with the following formula: $k_w = a_w + \beta_w$
Extinction coefficient of heavy metal	k_{HM}	Obtained from Ref. [5] for $CuSO_4$ solutions, while Ref. [7] for CdS solutions
Scattering coefficient of heavy metal	β_{HM}	Calculate with the following formula: $\beta_{HM} = R_{HM} \cdot k_{HM}$, where R_{HM} is the reflectance of the heavy metal, obtained from Ref. [7] for CdS solution. We take $\beta_{HM} \approx 0$ for $CuSO_4$ solutions in this paper
Total extinction coefficient of the other components in the background water except the heavy metal	K	Calculate with the following formula: $K = k_w$, taking the theoretical clear and deep water as an example
Total scattering coefficient of the other components in the background water except the heavy metal	B	Calculate with the following formula: $B = \beta_w$, taking the theoretical clear and deep water as an example
Reflectance of theoretical clear and deep water	R_w	Calculate with the following formula: $R_w = \frac{\beta_w P(\Theta)}{4\mu k_w}$, by Eq. (23)
Remote sensing image background DN value	DN_0	By Eq. (27)

therefore, the display range of Figure 2(a) is also enlarged to that shown in Figure 2(b).

Figure 3 shows the calculation results of the CdS solutions. Normal coordinates in the range from 0 to 0.25 mg/L, see Figure 3(a); for normal coordinates in the display range from 0 to 0.002 mg/L, see Figure 3(b); and for logarithmic coordinates, see Figure 3(c).

Using Eq. (24), the concentration sequences $\{D_1, D_2, \ldots, D_n\}$ of $CuSO_4$ and CdS can be obtained (see Figures 4 and 5). Figure 4 shows the calculation results of the $CuSO_4$ solutions. As a function of wavelength, concentration sequences $\{D_1, D_2, D_3, D_4, D_5, D_6, D_7, D_8, D_9, D_{10}\}$ with a sampling interval of 1 are shown in Figure 4(a); concentration sequences $\{D_1, D_3, D_5, D_7, D_9, D_{11}, D_{13}, D_{15}, D_{17}, D_{19}\}$ with a sampling interval of 2 are shown in Figure 4(b); concentration sequences $\{D_1, D_8, D_{15}, D_{22}, D_{29}, D_{36}, D_{43}, D_{50}, D_{57}, D_{64}\}$, which has a sampling interval of 7 are shown in Figure 4(c); and concentration sequences $\{D_1, D_{11}, D_{21}, D_{31}, D_{41}, D_{51}, D_{61}, D_{71}, D_{81}, D_{91}\}$, which have a sampling interval of 10 are shown in Figure 4(d). We actually calculated more than one hundred such curves, but the curves would be too dense to be displayed within a single graph; therefore, 10 curves are displayed with four different sampling intervals Figures 4(a) to 4(d) in order to show the results more clearly.

Figure 5 shows the calculation results of the CdS solutions. As a function of wavelength, concentration sequences $\{D_1, D_2, D_3, D_4, D_5, D_6, D_7, D_8, D_9, D_{10}\}$, which has a sampling interval of 1 are shown in Figure 5(a); concentration sequences $\{D_1, D_6, D_{11}, D_{16}, D_{21}, D_{26}, D_{31}, D_{36}, D_{41}, D_{46}\}$, which has a sampling interval of 5 are shown in Figure 5(b); concentration sequences $\{D_1, D_{21}, D_{41}, D_{61}, D_{81}, D_{101}, D_{121}, D_{141}, D_{161}, D_{181}\}$, which has a sampling interval of 20 are shown in Figure 5(c); and concentration sequences $\{D_1, D_{101}, D_{201}, D_{301}, D_{401}, D_{501}, D_{601}, D_{701}, D_{801}, D_{901}\}$, which has a sampling interval of 100 are shown in Figure 5(d).

3.2. The relationships revealed by the models

3.2.1. δ-ε Model

Eq. (5) defines the δ function, whose physical meaning is the ratio of the reflectance of the remote sensing images for two different concentrations. The principle of the sensitivity analysis is that the pixel values of the remote sensing images can distinguish two different situations, thus, it is necessary to consider the changes in the respective pixel values and reflectance in those two situations. Therefore, by first defining the ratio function, a relationship between the concentration and the radiometric

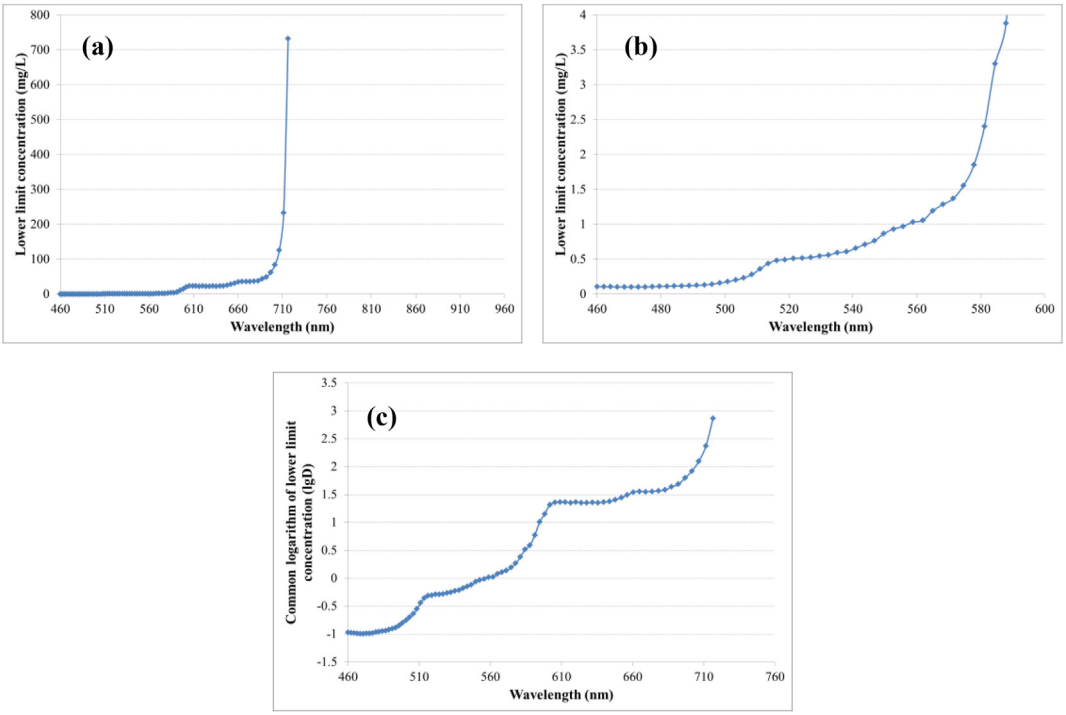

Figure 2. The curves for the lower limit concentrations that can be retrieved from remote sensing images of $CuSO_4$ solutions in the ideal clear and deep water in the HSI image band range.

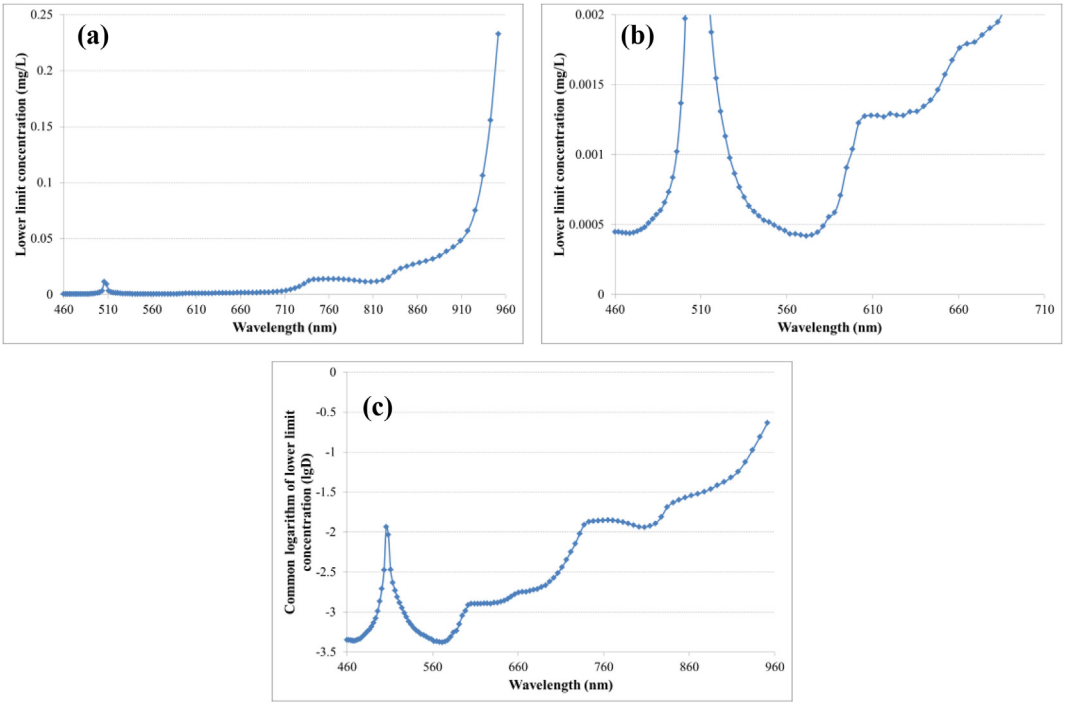

Figure 3. The curves for the lower limit concentrations that can be retrieved from remote sensing images of CdS solutions in the ideal clear and deep water in the HSI image band range.

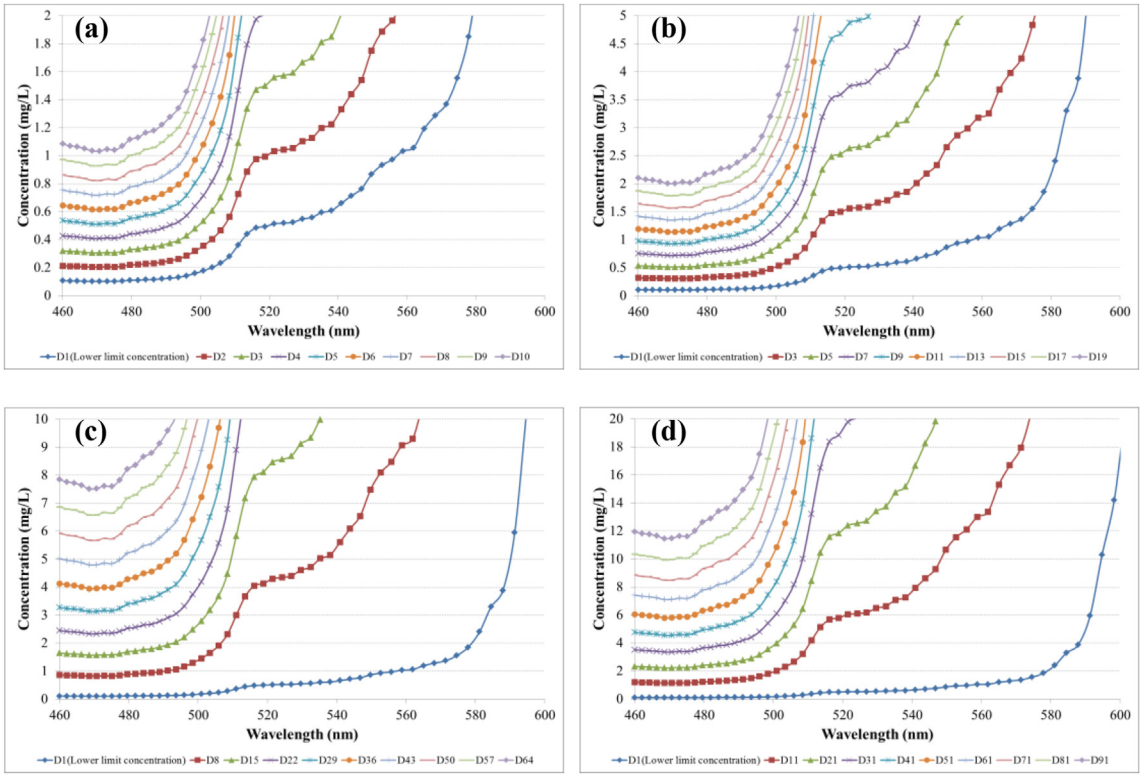

Figure 4. The curves for the concentration sequences (D_i) that can be retrieved from remote sensing images of $CuSO_4$ solutions in the ideal clear and deep water in the HSI image band range.

resolution is established. Furthermore, by defining the δ function, many of the derivations then become the operations within the sequence subscript. Compared with the direct derivations of the concentration and radiometric resolution, the model processes and expression forms are more concise and easier to understand.

Eq. (15) is the recursion formula of the δ function sequences. It can be found that the δ function is different for any two concentrations. The difference between the reflectance values is relatively large at the beginning, but will eventually become stabilize so that it satisfies:

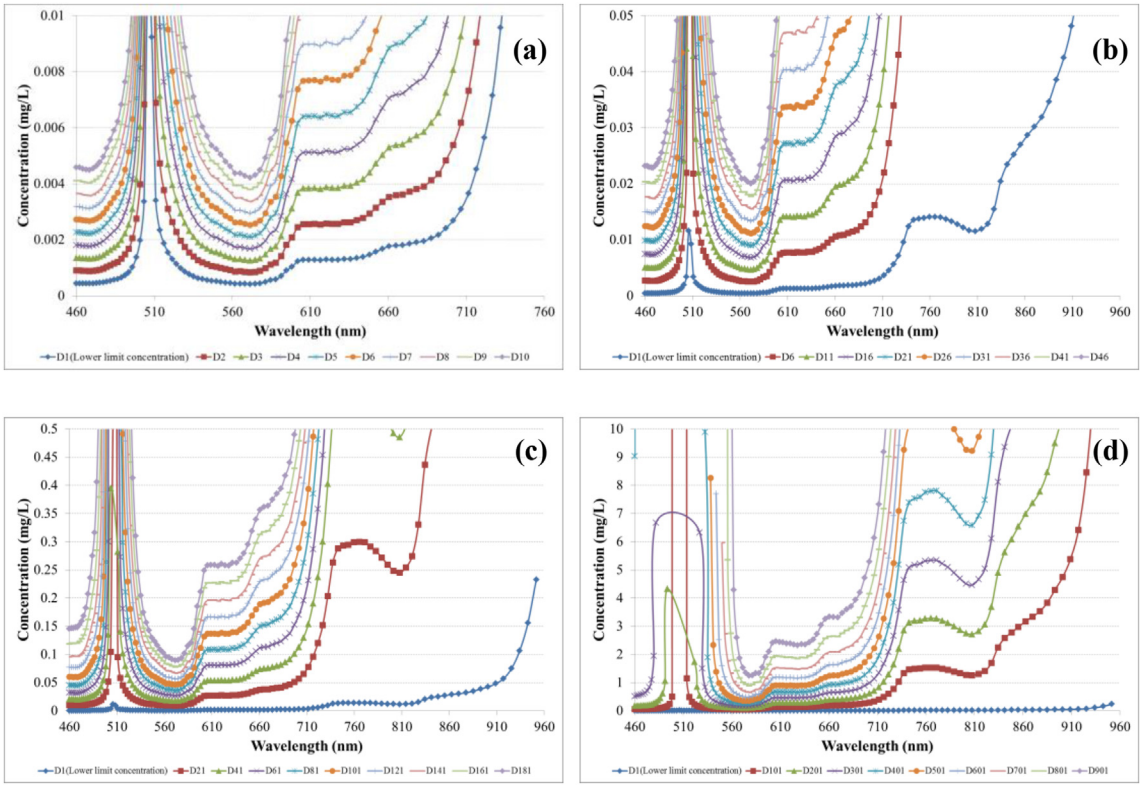

Figure 5. The curves for the concentration sequences (D_i) that can be retrieved from remote sensing images of CdS solutions in the theoretical clear and deep water in the HSI image band range.

$$\lim_{n\to+\infty}\delta_1(\varepsilon,n+1,n)=1.$$

Eq. (16) is the formula of the general term of the δ function sequences. It reflects the ratio between the initial reflectance and the reflectance at a certain concentration. Eq. (16) reveals the following relationships:

(1) If $\varepsilon>0$, $DN_0-n\cdot\varepsilon>0$ should also be satisfied, thus, $0<n<DN_0/\varepsilon$. When n takes the largest positive integer in this range, the reflectance will reach a minimum value (the lower limit of the pixel value). Therefore increasing n beyond this point is meaningless. Additionally, the δ function will tend to infinity, indicating that the reflectance is decreasing:

$$\lim_{n\to+DN_0/\varepsilon}\delta_n(\varepsilon,n,0)=+\infty.$$

(2) If $\varepsilon<0, DN_0-n\cdot\varepsilon\le 2^m-1$ should also be satisfied, thus $0<n\le(DN_0-2^m+1)/\varepsilon$. When n takes the largest positive integer in this range, the reflectance will reach a maximum value (the upper limit of the pixel value). Therefore, increasing n beyond this value is meaningless. Additionally, if the upper limit of the pixel value is not considered, the δ function will tend to 0, indicating that the reflectance is increasing:

$$\lim_{n\to+\infty}\delta_n(\varepsilon,n,0)=0.$$

The form of δ function indicates that at it is essentially a first order fractional function. One end of such a function tends toward infinity near the asymptote, and the other end tends toward 0, which correctly reflects the trend of reflectance changes in the above two situations.

3.2.2. D-δ(ε) Model

Eq. (24) shows that the concentration of heavy metals observed by satellite sensors at a certain wavelength is a discrete sequence {D_1, D_2, …, D_n}, and the concentration interval (somewhat similar to concentration resolution) between the increase from a certain concentration to the next concentration that can be observed is constantly changing.

Eq. (26) is regarded as the formula of the general term of the concentration sequences. It can be seen that at the beginning, the concentrations are nearly equal, which is indicative of an arithmetic progression. However, as n continues to increase, this concentration difference increases sharply and tends to infinity, thus it cannot be observed.

Eq. (25) is a special case of Eqs. (24) and (26) and has great value. This formula represents the minimum aqueous concentration value of heavy metals that can theoretically be observed by sensors, that is, the lower limit of the remote sensing retrieval. Eq. (25) indicates the following relationships:

(1) The lower concentration limit is related to the background optical parameters of the water, the optical parameters of the heavy metals and the radiometric resolution of the detection instrument. Since the optical parameters are inherent to the environment, they cannot be changed, i.e., inherent optical parameters (IOP).

To improve the detection capability in the future, it is necessary to start from the performance of the instrument and continuously improve its radiometric resolution. This is because when $|\varepsilon|$ is smaller, D_1 is smaller, i.e., the sensitivity is higher. Generally, for satellite images, $|\varepsilon|$ is reflected in the DN value, which is an integer, and the theoretical minimum change is 1 ($|\varepsilon|=1$). For ground based spectral measurement instruments, such as Analytical Spectral Devices FieldSpec 4 (ASD FS4), $|\varepsilon|$ is reflected in radiance (equivalent noise radiation, $|\varepsilon|=0.01W\cdot m^{-2}\cdot sr^{-1}\cdot\mu m^{-1}$).

(2) The background optical properties of the water affect the D_1 value. In the case of ideal clear and deep water that ignores the atmospheric effects, D_1 can be regarded as the theoretical minimum and lower concentration limit that can be retrieved from remote sensing images. However, as the optical parameters of the water

continue to increase, D_1 also increases, indicating that the sensitivity is decreasing.

(3) The optical parameters of the heavy metal itself also affect the D_1 value. When the extinction coefficient of the heavy metal is larger, the D_1 value will decrease instead, and the sensitivity will increase.

Therefore, the spectral characteristics of the optical parameters of the water components are the theoretical basis to guide us to select sensitive bands in the future.

3.2.3. Positive and negative discriminant conditions for ε

According to definition (4), the minimum change in the DN value of the remote sensing image can be either positive or negative. When $\varepsilon > 0$, it means that the DN value is decreasing and tending to 0; When $\varepsilon < 0$, it means that the DN value is increasing and tending to the maximum value of the pixel. For example, HSI images are 16 bit, so the theoretical maximum DN value is 65535. The following will deduce the conditions that should be satisfied for ε to appear positive or negative.

When $\varepsilon < 0$, according to Eq. (23), and $R_n/R_{n+1} < 1$, which means that the DN value continually increases, we obtain:

$$\frac{B + D_n\beta_{HM}}{K + D_n k_{HM}} \cdot \frac{K + D_{n+1}k_{HM}}{B + D_{n+1}\beta_{HM}} < 1 \tag{28}$$

$$(B + D_n\beta_{HM})(K + D_{n+1}k_{HM}) < (K + D_n k_{HM})(B + D_{n+1}\beta_{HM}) \tag{29}$$

$$Bk_{HM}(D_{n+1} - D_n) < K\beta_{HM}(D_{n+1} - D_n) \tag{30}$$

Since $D_{n+1} - D_n > 0$, we obtain:

$$\beta_{HM}/k_{HM} > B/K \tag{31}$$

Similarly, when $\varepsilon > 0$, and $R_n/R_{n+1} > 1$, which means that the DN value continually decreases, we obtain:

$$\beta_{HM}/k_{HM} < B/K \tag{32}$$

Eqs. (31) and (32) imply that the proportion of the scattering relationship between a certain heavy metal and the background water determines the increasing or decreasing trend of DN values. If the scattering proportion of heavy metals is greater than that of the background water, the DN value will increase as the concentration increases, and vice versa. The scattering of some dissolved heavy metal compounds (such as copper ions) usually occurs at the molecular level, and its effects are much lower than the absorption, that is, $\beta_{HM} \approx 0$. The situation of Eq. (31) does not exist, and only Eq. (32) can be applied, which indicates that the DN value can only be gradually reduced.

The significance of Eqs. (31) and (32) is that the above two situations may occur in the concentration sequences at different observation wavelengths, and they are the discriminant formulas that should be considered first before calculating the lower limit concentration.

3.3. Results and discussion

$CuSO_4$ exists in a dissolved state in water, while CdS exists in a particulate state, so this paper takes these two different physicochemical properties as a representative example of sensitivity analysis.

3.3.1. Remote sensing sensitivity analysis of $CuSO_4$ in water

Figures 2(a) and 2(b) show that the lowest concentration of $CuSO_4$ that can be retrieved from remote sensing images varies with wavelength. Figure 2(c) shows that the concentration can span four orders of magnitude, and the sensitivity varies greatly with different observation wavelengths. From the results, we found that the lowest concentration appears at a wavelength of 470.705 nm (corresponding to Band 6 of the HSI image), which corresponds to 0.1013 mg/L and is theoretically the most sensitive wavelength for detecting this compound in water via remote sensing. That is, in theory, as long as the concentration in water reaches 0.1013 mg/L or more, it can be observed by remote sensing imaging. In addition, within the range of the central wavelengths (460.04–496 nm, or Bands 1–17), the lowest detectable concentration is lower than 0.15 mg/L. These are relatively sensitive bands that can be considered in the future. In contrast, for wavelengths in the range of 721.605–951.54 nm (Band 81–115), there is no lower concentration limit since the reflectance of the water is close to zero, That is, no matter how much the concentration increases, the DN value cannot be changed, and these bands are ineffective for remote sensing retrieval. For compounds such as $CuSO_4$ solutions with high absorptivity, the surface reflectance of the Earth can only gradually decrease as the concentration increases, thus, it is almost impossible to effectively use remote sensing methods in waters with extremely low background reflectance.

Figure 6 shows the concentration sequences D_i at several wavelengths (somewhat similar to the concentration resolution, $i = 100$). It can be found that the concentration spacing is almost equal at the beginning, which is approximately an arithmetic sequence, but as it increases, the concentration will increase sharply. This shows that it is difficult to change the DN value at higher concentrations, and the sensitivity gradually decreases. From Figure 6, for example, we take 0.2 mg/L as the threshold. If we choose the wavelength of 479.6 nm (Band 10, Figure 6(■)), 100 different concentrations can be distinguished, but if we choose the wavelength of 568.16 nm (Band 43, Figure 6(●)), only 8 different concentrations can be distinguished, and the concentration resolution drops sharply. Therefore, it is very important to select a suitable band for remote sensing retrieval.

3.3.2. Remote sensing sensitivity analysis of CdS in water

Figure 3(b) shows that the theoretically lowest retrievable limit of the CdS concentration is 0.00042 mg/L at a wavelength of 571.36 nm (Band 44). In the separate ranges of 460.04–493.59 nm (Band 1–16) and 526.885–594.79 nm (Band 29–51), the lower limit concentrations were lower than 0.001 mg/L. The lower concentration limits can vary by several orders of magnitude from 10^{-4} to 10^{-1}, indicating that the sensitivity of the different wavelengths is also very different.

Since CdS is a granular compound, its scattering effect cannot be ignored. Therefore, before calculating D_1, we must first assess Eqs. (28) and (29) to determine the positive or negative value of ε. Figure 7 shows that the scattering proportion of the background water at 460.04–505.885 nm (Bands 1–21) is larger than that of heavy metals, which is consistent with Eq. (32). The image DN value at these wavelengths decreases with increasing concentration and tends to 0, while the scattering proportion of the background water at 508.42–951.54 nm (bands 22–115) is lower than that of heavy metals, which is consistent with Eq. (31). The image DN value at these wavelengths increases with increasing concentration and tends to the maximum pixel value of 65535. Due to its strong backscattering, the sensor can receive this part of the energy; therefore, it can still be used for retrieval even in the near-infrared band, which is strongly absorbed by water. However, for wavelengths greater than 925.52 nm (Band 112), the lower concentration limit increases rapidly, and the sensitivity decreases.

3.4. The limitations and influencing factors of this method

Applications of the D-δ(ε) model we constructed needs to consider to the following aspects:

(1) The radiometric resolution is a physical characteristic of the sensor. For example, the radiometric resolution of the satellite data is reflected in the DN value, but ground spectrometers indicate radiance. The mathematical form of the model will thus be slightly different.

(2) When applied to real satellite data, atmospheric effects should be considered and appropriate atmospheric correction models should

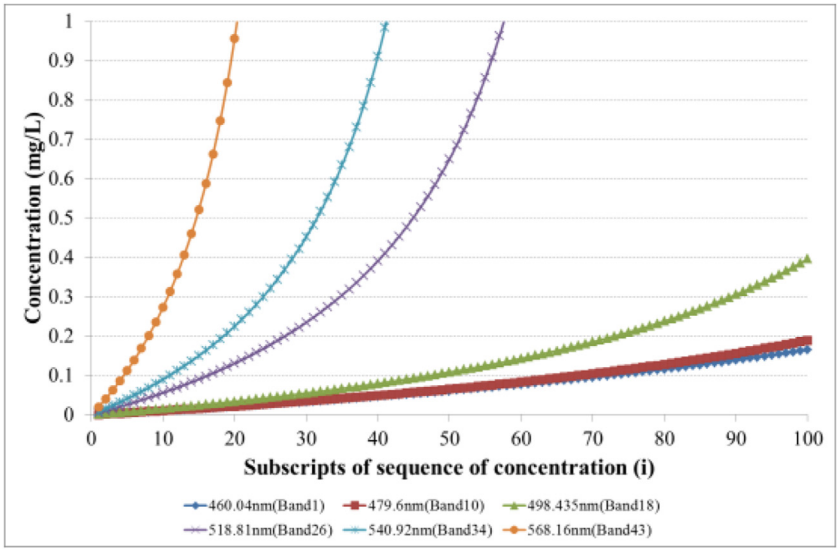

Figure 6. Concentration sequences D_i (i = 100) at 460.04 nm (Band 1), 479.6 nm (Band 10), 498.435 nm (Band 18), 518.81 nm (Band 26), 540.92 nm (Band 34), 568.16 nm (Band 43) wavelengths.

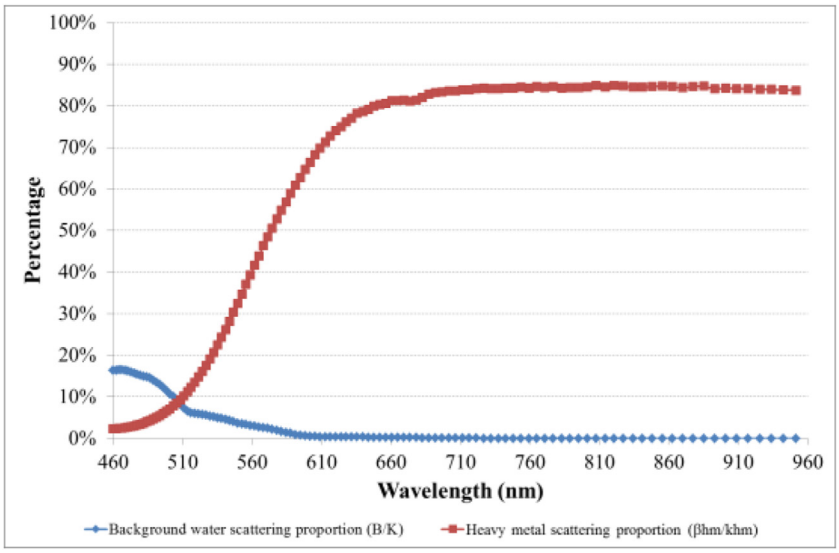

Figure 7. Scattering proportion of background water and CdS as a function of wavelength.

be used, such as the Fast Line of sight Atmospheric Analysis of Spectral Hypercubes (FLAASH) and Dark-Object Subtraction (DOS). Furthermore, planetary reflectance must be converted to surface reflectance of the Earth before application.

(3) For sensitivity analyses that need to consider multiple components at the same time, this method can still be used because the parameters that characterize the water were set as variables when the model is constructed. In the case of multiple components, this is equivalent to carrying out sensitivity analyses in the water that already contains one or several components.

(4) It is the objective of this method to solve the mathematical analytical expression of the g function in equations (18) ~ (21). Therefore, the water quality remote sensing model (f_1) and the atmospheric correction model (f_2) should be expressed algebraically. In the case of transcendental equations, the g function in the model can only be expressed implicitly. It is necessary to use a numerical approximation method to estimate the transcendental equation for conversion into an algebraic equation before continuing to use this method.

4. Conclusions

The remote sensing sensitivity analysis model for heavy metals in water (the D-δ(ε) model) developed in this study clearly reveals the mathematical relationship between the concentration of heavy metals retrieved from remote sensing and the radiometric resolution of the satellite sensors. Two heavy metal compounds, $CuSO_4$ and CdS, are taken as examples to demonstrate the advantages of this model in the selection of sensitive bands for remotely sensing heavy metals in water. The research results can mitigate the doubts of the academic community about the feasibility of this remote sensing application.

Theoretically, the model reveals a clear functional relationship between the concentration of heavy metals that can be retrieved by remote sensing and the optical parameters of the water and the radiometric resolution of the satellite sensors. Specifically, the lower limit of the detectable concentration is positively correlated with the radiometric resolution and the background value of the water optical parameters, but is negatively correlated with the optical parameters of heavy metals. The model is developed from these relationships and has strong universality.

Furthermore, the model is independent of the retrieval parameter to be subjected to the sensitivity analysis, which can be any nonheavy metal parameter such as ammonia nitrogen, total phosphorus, and total nitrogen (as long as their optical parameters are measured). Additionally, the model is also independent of the sensor type and can be used not only for HJ-1A HSI data, such as in this study but also for Landsat images, Sentinel 2 images, ASD spectrometer measurement data, etc.

In application, the resolvable concentration of each detection band is quantitatively given, and the lower detection limits at the different wavelengths are usually very different. Therefore, the model results provide a theoretical basis for selecting sensitive bands. Sometimes, the theoretical minimum value calculated by the model is still a relatively large value for the heavy metal concentrations of natural water. However, we can use the model to inversely calculate the radiometric resolution of the spectral detection sensors based on the background heavy metal concentrations of natural water. This provides a useful reference threshold for radiometric resolution when designing new instruments in the future.

Therefore, the model we constructed quantitatively determines the curve of the lowest detectable limits of heavy metal concentrations retrieved by remote sensing methods as a function of wavelength. This provides a strong theoretical basis for selecting sensitive bands in future remote sensing retrieval studies. This model has important scientific significance and application value and promotes the further development of the field of remote sensing for the monitoring of heavy metals in water.

Declarations

Author contribution statement

Yu Guo; Yeheng Liang: Conceived and designed the experiments; Performed the experiments; Wrote the paper.

Ruru Deng: Conceived and designed the experiments; Contributed reagents, materials, analysis tools or data.

Jiayi Li; Jing Wang; Zhenqun Hua; Yuming Tang: Analyzed and interpreted the data.

Funding statement

Dr. Yeheng Liang was supported by National Natural Science Foundation of China [41901352], Basic and Applied Basic Research Foundation of Guangdong Province [2020A1515010780], Science and Technology Projects of Guangzhou City [202102020454].

Prof. Ruru Deng was supported by National Natural Science Foundation of China [41071230].

Data availability statement

Data included in article/supp. material/referenced in article.

Declaration of interest's statement

The authors declare no conflict of interest.

Additional information

No additional information is available for this paper.

References

[1] C. Chen, F. Liu, Q. He, H. Shi, The possibility on estimation of concentration of heavy metal in coastal waters from remote sensing data, IEEE Int. Symp. Geosci. Remote Sens. IGARSS (2010) 4216–4219.

[2] C. Chen, F. Liu, S. Tang, Estimation of heavy metal concentration in the pearl river estuarine waters from remote sensing data, IEEE Int. Symp. Geosci. Remote Sens. IGARSS (2012) 2575–2578.

[3] F. Liu, S. Tang, C. Chen, Estimation of particulate zinc using MERIS data of the pearl river estuary, Remote Sens. Lett. 4 (8) (2013) 813–821.

[4] Y. Liang, R. Deng, Y. Wu, Y. Qin, A research of remote sensing inversion for heavy metal Cu and Fe in nature water using HJ-1A HSI data——a case study of Beijiang basin in Guangdong province. 7th Heavy Metal Pollut Prevention Technol Risk, Assess Semin. (2017) 227–235.

[5] Y. Liang, R. Deng, Y. Gao, Y. Qin, X. Liu, Measuring the absorption coefficient spectrum (400–900nm) of copper ion in water, J. Remote Sens. 20 (1) (2016) 27–34.

[6] R. Deng, Y. Liang, Y. Gao, Y. Qin, X. Liu, Measuring absorption coefficient spectrum (400–900nm) of hydrated and complex ferric ion in water, J. Remote Sens. 20 (1) (2016) 35–44.

[7] Y. Liang, R. Deng, Y. Liu, L. Lin, Y. Qin, Y. He, Measuring the spectrum of extinction coefficient and reflectance for cadmium compounds from 400 to 900 nm, Spectrosc. Spectr. Anal. 36 (12) (2016) 4006–4012.

[8] Y. Liang, R. Deng, J. Huang, L. Xiong, Y. Qin, Z. Liu, The spectral characteristic analysis of typical heavy metal polluted water——a case study of mine drainage in Dabaoshan mountain, Guangdong province, China, Spectrosc. Spectr. Anal. 39 (10) (2019) 3237–3244.

[9] Y. Liang, R. Deng, Y.J. Liang, Y. Liu, Y. Wu, Y. Yuan, X. Ai, Spectral characteristics of sediment reflectance under the background of heavy metal polluted water and analysis of its contribution to the water-leaving reflectance, Spectrosc. Spectr. Anal. (2022) in press.

[10] Y. Cheng, Y. Li, F. Ji, Y. Wang, Global sensitivity analysis of a water quality model in the three gorges reservoir, Water 10 (2) (2018) 153.

[11] H. Jia, T. Xu, S. Liang, P. Zhao, C. Xu, Bayesian framework of parameter sensitivity, uncertainty, and identifiability analysis in complex water quality models, Environ. Model. Software 104 (2018) 13–26.

[12] X. Yi, R. Zou, H. Guo, Global sensitivity analysis of a three-dimensional nutrients-algae dynamic model for a large shallow lake, Ecol. Model. 327 (2016) 74–84.

[13] Y. Wang, Z. Hua, L. Wang, Sensitivity analysis of the Chaohu lake eutrophication model with a new index based on the morris method, Water Supply 18 (4) (2018) 1375–1387.

[14] G. Li, L. Li, G. Li, Spatial-temporal parameter sensitivities of the Dianchi algae model based on EFDC, Chin. J. Appl. Environ. Biol. 4 (27) (2021) 1047–1054.

[15] L. Liu, Q. Jiang, G. Mao, Y. Liu, Global sensitivity analysis of parameters and boundary conditions to water quality model in lake Dianchi, Acta Sci. Circumstantiae 5 (42) (2022) 384–394.

[16] P. Vanrolleghem, G. Mannina, A. Cosenza, M. Neumann, Global sensitivity analysis for urban water quality modelling: terminology, convergence and comparison of different methods, J. Hydrol. 522 (2015) 339–352. Global sensitivity analysis for urban water quality modelling: terminology, convergence and comparison of different methods.

[17] D.S. Ikumi, Sensitivity analysis on a three-phase plant-wide water and resource recovery facility model for identification of significant parameters, WaterSA 46 (3) (2020) 476–492.

[18] M. Mbuh, R. Mbih, C. Wendi, Water quality modeling and sensitivity analysis using water quality analysis simulation program (WASP) in the shenandoah river watershed, Phys. Geogr. 40 (2) (2019) 127–148.

[19] C. Manzo, M. Bresciani, C. Giardino, F. Braga, C. Bassani, Sensitivity analysis of a bio-optical model for Italian lakes focused on landsat-8, sentinel-2 and sentinel-3, Eur. J. Remote Sens. 48 (1) (2017) 17–32.

[20] L. Soares, M. Calijuri, Sensitivity and identifiability analyses of parameters for water quality modeling of subtropical reservoirs, Ecol. Model. 458 (2021), 109720.

[21] S. Xu, G. He, H. Fang, S. Bai, X. Wu, Parameter uncertainty and sensitivity analysis of the three gorges reservoir and Xiangxi river EFDC model, J. Hydrol. 610 (2022), 127881.

[22] N. Hosseini, K. Chun, H. Wheater, K. Lindenschmidt, Parameter sensitivity of a surface water quality model of the lower south saskatchewan river—comparison between ice-on and ice-off periods, Environ. Model. Assess. 22 (4) (2017) 291–307.

[23] J. Privette, R. Myneni, W. Emery, F. Hall, Optimal sampling conditions for estimating grassland parameters via reflectance, IEEE Trans. Geosci. Rem. Sens. 34 (1) (1996) 272–284.

[24] X. Li, F. Gao, J. Wang, Q. Zhu, Uncertainty and sensitivity matrix of parameters in inversion of physical BRDF model, J. Remote Sens. 1 (1) (1997) 5–14.

[25] Y. Yao, Q. Liu, Q. Liu, X. Li, Research on the mutual effect of the parameters on inversion of canopy reflectance model, J. Remote Sens. 12 (1) (2008) 1–8.

[26] N. Hosseini, K. Chun, K. Lindenschmidt, Quantifying spatial changes in the structure of water quality constituents in a large prairie river within two frameworks of a water quality model, Water 8 (4) (2016) 158.

[27] L. Chen, Z. Yang, H. Liu, Sensitivity analysis for the total nitrogen pollution of the Danjiangkou reservoir based on a 3-d water quality model, Front. Earth Sci. 11 (4) (2017) 609–619.

[28] E. Ustinov, Adjoint sensitivity analysis of radiative transfer equation: 2. Applications to retrievals of temperature in scattering atmospheres in thermal IR, J. Quant. Spectrosc. Radiat. Transf. 73 (1) (2002) 29–40.

[29] E. Ustinov, Adjoint sensitivity analysis of atmospheric dynamics: application to the case of multiple observables, J. Atmos. Sci. 58 (21) (2001) 3340–3348. ASAOAD>2.0.CO;2.

[30] E. Ustinov, Adjoint sensitivity analysis of radiative transfer equation: temperature and gas mixing ratio weighting functions for remote sensing of scattering atmospheres in thermal IR, J. Quant. Spectrosc. Radiat. Transf. 68 (2) (2001) 195–211.

[31] R. Deng, Q. Liu, R. Ke, L. Chen, X. Liu, Model for water pollution remote sensing based on double scattering and its application in the Zhujiang river outfall, Acta Oceanol. Sin. 23 (1) (2004) 119–128.

[32] R. Deng, Y. He, Y. Qin, Q. Chen, L. Chen, Pure water absorption coefficient measurement after eliminating the impact of suspended substance in spectrum from 400 nm to 900 nm, J. Remote Sens. 16 (1) (2012) 174–191.

[33] R. Deng, Y. He, Y. Qin, Q. Chen, L. Chen, Measuring pure water absorption coefficient in the near-infrared spectrum (900—2500nm), J. Remote Sens. 16 (1) (2012) 192–198.

[34] R. Smith, K. Baker, Optical properties of the clearest natural waters (200–800 nm), Appl. Opt. 20 (2) (1981) 177–184.